Bulletin of the JSME Vol.2, No.2, 2015
Mechanical Engineering Journal

# Analysis for fluid-elastic instability of tube arrays in cross-flow

Masahiko UTSUMI*
* Machine Element Department, Technical Research Laboratory, IHI Corporation
1, Shin-Nakahara-cho, Isogo-ku, Yokohama-shi, Kanagawa 235-8501, Japan
E-mail: masahiko_utsumi@ihi.co.jp

**Received 3 September 2014**

**Abstract**
To date, no study has been conducted on analytical methods to solve the fluid dynamics governing equations system for the fluid-elastic vibration of tube arrays in a straightforward manner. In this paper, a semi-analytical method for this vibration problem is investigated by considering the system as a collection of regular polygon cells and expressing unknowns on each side of the cells by base expansion. Based on this expression, the solutions in the cell are expressed in terms of polar coordinates, allowing for circumferential variation in the radial coordinate interval. Via this means, a reduced-order model is developed for the tube array-fluid system and the proposed method is verified by comparing with earlier experimental results.

***Key words***: Fluid-elastic instability, Tube array, Cross-flow, Semi-analytical method, Critical flow velocity

## 1. Introduction

The determination of critical flow velocity for the threshold of fluid-elastic instability of a tube array in cross-flow has been an important research topic for tube-in-shell heat exchangers (Paidoussis, 1983; Price, 1995; Weaver et al., 2000). Methods widely used express the fluid-force components acting on a certain tube in terms of a linear combination of the motions of the neighboring tubes and identify the coefficients experimentally to conduct stability analysis (Tanaka et al., 2002; Chen, 1983a, 1983b; Khulief et al., 2009; Yetisir and Weaver, 1993a, 1993b; Price and Paidoussis, 1984; Granger and Paidoussis, 1996). Other studies applied a one-dimensional channel flow approximation (Lever and Weaver, 1982), computer fluid dynamics (CFD) approaches (Kassera and Strohmeier, 1997; Ichioka et al., 1997), and experimental methods (Weaver and Grover, 1978; Mureithi et al., 2005; Violette et al., 2005) to predict the critical flow velocity. However, no analytical method has been investigated that solves the fluid dynamics governing equations system for a tube array's fluid-elastic vibration in a straightforward manner. This is due to the geometrical complexity of the fluid domain among the tubes. In this paper, a semi-analytical method for solving this vibration problem is studied. In this method, the system is considered to constitute a collection of regular polygon cells, with the unknowns on each side of the cells expressed by base expansion. Next, polar coordinate expressions of the solutions in each cell are derived by allowing for circumferential variation in the radial coordinate interval. This method reduces the number of degrees of freedom and computational efforts compared to conventional numerical methods. The proposed method is verified by comparing with earlier experimental results. Furthermore, theoretical predictions are made for instability in the flow direction induced in rotated triangular tube arrays; studies for which are scarce and for which few experimental works exist, despite its practical importance (Mureithi et al., 2005; Violette et al., 2005).

## 2. Nomenclature

$A_{1n}$ - $A_{3n}$ : generalized coordinates of basic flow velocities ($V_x$, $V_y$) and pressure $P$ on each side of the cell
$a_{1n}$ - $a_{3n}$ : generalized coordinates of vibrational flow velocities ($v_x$, $v_y$) and pressure $p$ on each side of the cell

Paper No.14-00377
J-STAGE Advance Publication date : 24 February, 2015
[DOI: 10.1299/mej.14-00377]

$a$ : outer radius of tubes
$B_{1mqk}$ - $B_{3mqk}$ : generalized coordinates of basic flow velocities ($V_x$, $V_y$) and pressure $P$ in cell
$b_{1mqk}$ - $b_{3mqk}$ : generalized coordinates of vibrational flow velocities ($v_x$, $v_y$) and pressure $p$ in cell
$C$ : damping coefficient introduced into the bulk modulus $K$
$D$ : distance between the center and each side of the cell
$d$ : outer diameter of tubes ($2a$)
e : base of natural logarithm
$F_{\mathrm{vis}}$ : viscous force acting on tubes
$\mathbf{G}$ : nonlinear term in an ordinary time-differential equation for basic flow
$h_1, h_2$ : functions for interpolation on the side of the cell
$h_{3n}$ : base function on the side of the cell
i : imaginary unit
$i$ : index number of apexes of the cells
$K$ : bulk modulus corresponding to artificial compressibility used for time-domain analysis of fluid-governing equations
$k$ : base function index for radial direction in the cell
$m$ : circumferential wave number of fluid motion in the cell
$\overline{m}$ : base function index for circumferential direction in the cell
$m_b$ : mass of tube per unit length
$n$ : base function index for the side of the cell
$P$ : basic flow pressure at arbitrary positions
$\overline{P}$ : $P + p$
$P_i$ : basic flow pressure at apex $i$
$P_{\mathrm{out}}$ : basic flow pressure on the outer circumference of the cell
$\mathbf{P}_0$ : matrix in an ordinary time-differential equation for basic flow
$\mathbf{P}_1$ : matrix in an ordinary time-differential equation for stability analysis
$p$ : vibrational flow pressure at arbitrary positions
$p^{(m)}$ : main flow pressure just outside the boundary layer caused by tube vibration
$p_{BL}$ : pressure in the boundary layer due to tube vibration
$p_i$ : vibrational flow pressure at apex $i$
$p_{\mathrm{out}}$ : vibrational flow pressure along the outer circumference of the cell
$\mathbf{Q}_0$ : matrix in the ordinary time-differential equation for basic flow
$\mathbf{Q}_1$ : matrix in the ordinary time-differential equation for stability analysis
$q$ : base function index for the circumferential direction in the cell
$q_x, q_y$ : $x$ and $y$ tube displacement components
$Re$ : Reynolds number $2\rho V_c a / \mu$ for the basic flow considering increase in $\mu$ with increasing molecular viscosity-based Reynolds number
$\mathbf{R}_0$ : source term in the ordinary time-differential equation for the basic flow
$(r, \varphi)$ : polar coordinates for each cell
$r_{\mathrm{out}}$ : $\varphi$-dependent $r$ coordinate of the outer circumference of the cell
$s$ : coordinate defined along each side of the cell
$s_i$ : $s$ at apex $i$
$s_0$ : $s$ at which the distance between the center and each side of the cell is minimum
$T$ : pitch of the tube array
$t_0$ : time of basic flow solution used for stability analysis
$V_{\mathrm{c}}$ : velocity of the basic flow at clearance between tubes
$V_{\mathrm{reduc}}$ : reduced flow velocity $V_{\mathrm{c}} / 2\pi^{-1}\omega_x d$
$V_r, V_\varphi$ : $r$ and $\varphi$ basic flow velocity components in arbitrary positions
$V_{r,\mathrm{out}}, V_{\varphi,\mathrm{out}}$ : $r$ and $\varphi$ basic flow velocity components on the outer circumference of the cell
$\overline{V}_r, \overline{V}_\varphi$ : $V_r + v_r$ and $V_\varphi + v_\varphi$, respectively
$V_{\mathrm{src}}$ : source velocity for creating basic flow

[DOI: 10.1299/mej.14-00377]

$V_{x,i}$, $V_{y,i}$ : $x$ and $y$ basic flow velocity components at apex $i$
$V_{x,\mathrm{out}}$, $V_{y,\mathrm{out}}$ : $x$ and $y$ basic flow velocity components on the outer circumference of the cell
$v_r$, $v_\varphi$ : $r$ and $\varphi$ vibrational flow velocity components in arbitrary positions
$v_{r,\mathrm{out}}$, $v_{\varphi,\mathrm{out}}$ : $r$ and $\varphi$ vibrational flow velocity components on the outer circumference of the cell
$v_{x,i}$, $v_{y,i}$ : $x$ and $y$ vibrational flow velocity components at apex $i$
$v_{x,\mathrm{out}}$, $v_{y,\mathrm{out}}$ : $x$ and $y$ vibrational flow velocity components on the outer circumference of the cell
$v_\varphi^{(b)}$ : tangential velocity of the tube surface
$v_\varphi^{(m)}$ : main flow velocity just outside the boundary layer caused by tube vibration
$v_{\varphi,BL}$ : flow velocity in the boundary layer due to tube vibration
$(X,Y)$ : global Cartesian coordinates
$\mathbf{X}_0$ : unknown vector in the ordinary time-differential equation for basic flow
$\mathbf{X}_1$ : unknown vector in the ordinary time-differential equation for vibrational flow
$(x,y)$ : Cartesian coordinates for each cell
$\beta$ : artificial inertia coefficient
$\Delta t$ : time increment for basic flow analysis
$\varepsilon$ : 1 or $-1$ when $ds/d\varphi$ is positive or negative, respectively
$\zeta_b$ : damping ratio of tubes in air
$\mu$ : dynamic viscosity of fluid
$\nu$ : kinematic viscosity of fluid
$(\xi,\eta)$ : Cartesian coordinates to analyze the vibrational boundary layer flow
$\rho$ : fluid density
$\Phi_{mq}$ : $\cos m\varphi$ or $\sin m\varphi$ when $q$=1 or $q$=2, respectively
$\overline{\Phi}_{1\overline{m}}$ - $\overline{\Phi}_{3\overline{m}}$ : base function for basic flow in a rotated triangular tube array
$\varphi$ : circumferential coordinate in each cell
$\varphi_{\max}$, $\varphi_{\min}$ : maximum and minimum $\varphi$ in cell (basic flow analysis for triangular array)
$\varphi_0$ : $\varphi$ at which the distance between the center and each side of the cell is minimum
$\omega$ : frequency of boundary layer flow
$\omega_x$, $\omega_y$ : tube eigenfrequencies in $x$ and $y$ directions, respectively

Superscript
$\hat{A}$ : dimensionless quantity for $A$
$\tilde{A}$ : amplitude function for $A$

## 3. Analysis

### 3.1 Computational model

This study analyzes the cases of square array and rotated triangular array using square and regular hexagon cells, respectively (Fig. 1). A two-dimensional problem is considered, in which the phenomena are invariant along the direction normal to the cross-section shown in Fig. 1. For each cell, Cartesian and polar coordinates $(x,y)$ and $(r,\varphi)$ are defined as shown in Fig. 2 (the case of the rotated triangular array is shown as an example). A one-dimensional coordinate $s$ is defined along each side of the cell. The relation between $s$ and $\varphi$ is given by

$$s = s_0 + \varepsilon D \tan(\varphi - \varphi_0) \tag{1}$$

First the basic flow field is determined under the condition that the tubes are at rest (Sec. 3.2), whereupon the stability analysis is conducted by considering the vibrational components (Sec. 3.3).

### 3.2 Determination of the Basic Flow Field

#### 3.2.1 Expression of Solution by Base Expansion

In the present tube array analysis, the $x$ and $y$ components of the fluid velocity and the pressure on side $ij$ connecting apexes $i$ and $j$ (outer circumference of the cell) are expressed by linear interpolation and base expansion:

[DOI: 10.1299/mej.14-00377]

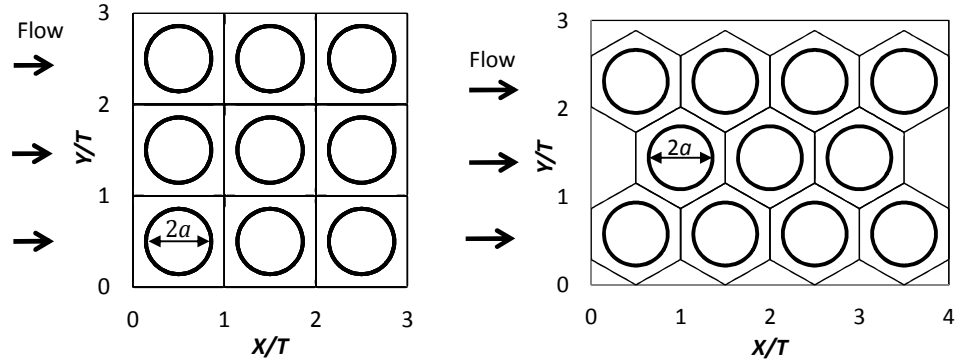


(a) Square tube array (b) Rotated triangular tube array

Fig. 1 Cross-sections of tube arrays

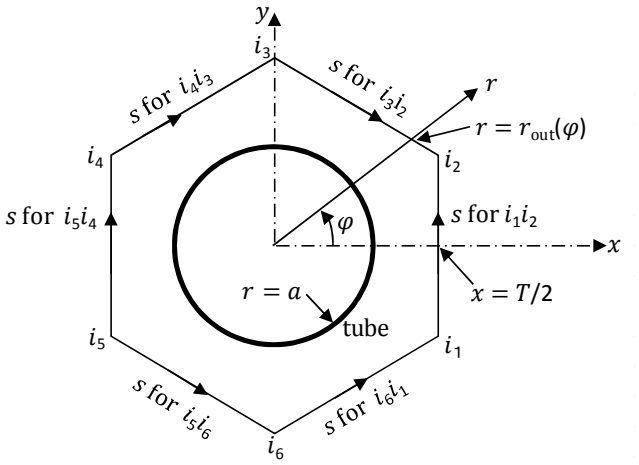


Fig. 2 Coordinate systems for one regular polygon cell (the case of the rotated triangular array is shown as an example)

$$\begin{Bmatrix} V_{x,\text{out}}(\varphi,t) \\ V_{y,\text{out}}(\varphi,t) \\ P_{\text{out}}(\varphi,t) \end{Bmatrix} = \begin{Bmatrix} V_{x,i}(t) \\ V_{y,i}(t) \\ P_i(t) \end{Bmatrix} h_1(s) + \begin{Bmatrix} V_{x,j}(t) \\ V_{y,j}(t) \\ P_j(t) \end{Bmatrix} h_2(s) + \sum_{n\geq 1} \begin{Bmatrix} A_{1n}(t) \\ A_{2n}(t) \\ A_{3n}(t) \end{Bmatrix} h_{3n}(s) \tag{2}$$

with

$$h_1(s) = \frac{s_j - s}{s_j - s_i}, \quad h_2(s) = \frac{s - s_i}{s_j - s_i}, \quad h_{3n}(s) = \sin\left[\frac{n\pi(s - s_i)}{s_j - s_i}\right] \tag{3}$$

The base expansion term is introduced to improve the linear interpolation approximation. Because the polar coordinates are convenient to analyze the fluid motion in each cell, we calculate $V_{r,\text{out}}$ and $V_{\varphi,\text{out}}$ from $V_{x,\text{out}}$ and $V_{y,\text{out}}$ using

$$\begin{Bmatrix} V_{r,\text{out}}(\varphi,t) \\ V_{\varphi,\text{out}}(\varphi,t) \end{Bmatrix} = \begin{Bmatrix} V_{x,\text{out}}(\varphi,t)\cos\varphi + V_{y,\text{out}}(\varphi,t)\sin\varphi \\ -V_{x,\text{out}}(\varphi,t)\sin\varphi + V_{y,\text{out}}(\varphi,t)\cos\varphi \end{Bmatrix} \tag{4}$$

and express the fluid velocity and pressure at arbitrary positions $(r,\varphi)$ as follows by allowing for the $\varphi$ - dependence of the radial coordinate interval $a \leq r \leq r_{\text{out}}$.

$$\begin{Bmatrix} V_r(r,\varphi,t) \\ V_\varphi(r,\varphi,t) \\ P(r,\varphi,t) \end{Bmatrix} = \begin{Bmatrix} V_{r,\text{out}}(\varphi,t) \\ V_{\varphi,\text{out}}(\varphi,t) \\ P_{\text{out}}(\varphi,t) \end{Bmatrix} \frac{r-a}{r_{\text{out}}-a} + \sum_{m\geq 0} \sum_{q=1,2} \sum_{k\geq 1} \begin{Bmatrix} B_{1mqk}(t)\sin[k\pi(r-a)/(r_{\text{out}}-a)] \\ B_{2mqk}(t)\cos[(2k-1)(\pi/2)(r-a)/(r_{\text{out}}-a)] \\ B_{3mqk}(t)\cos[(2k-1)(\pi/2)(r-a)/(r_{\text{out}}-a)] \end{Bmatrix} \Phi_{mq}(\varphi) \tag{5}$$

[DOI: 10.1299/mej.14-00377]

with

$$\Phi_{m1}(\varphi)=\cos m\varphi,\quad \Phi_{m2}(\varphi)=\sin m\varphi \tag{6}$$

The first term on the right-hand side of Eq. (5) vanishes at the inner circumference $r=a$ and matches the solution [Eq. (2)] at the outer circumference $r=r_{\text{out}}$. Therefore, the added base expansion term is introduced such that it vanishes at $r=r_{\text{out}}$ and that the velocity component normal to the tube surface vanishes, i.e. $V_r\big|_{r=a}=0$. The tangential velocity on the tube surface is not fixed to zero because the boundary layer is very thin. To allow for non-zero $V_\varphi$ and $P$ at $r=a$, their base expansion terms do not vanish at $r=a$.

The generalized coordinates $A_{1n}$ - $A_{3n}$ are defined for each side of the cell while the generalized coordinates $B_{1mqk}$ - $B_{3mqk}$ are introduced for each cell (tube).

The $r$- and $\varphi$-coordinates are convenient to analyze the fluid motion in each cell. However, to express the fluid velocity on the outer circumference of the cells, the $x$- and $y$-coordinates are more convenient because the $r$- and $\varphi$-directions depend on the cells. For this reason, this analysis uses the Cartesian coordinates as well as the polar coordinates.

By substituting Eq. (2) into (4) and inserting the resulting equation into Eq. (5), the fluid velocity and pressure in arbitrary positions can be expressed in terms of the fluid velocity and pressure at the apexes and the generalized coordinates $A_{1n}$ - $A_{3n}$ and $B_{1mqk}$ - $B_{3mqk}$ as follows:

$$\begin{Bmatrix} V_r(r,\varphi,t)\\ V_\varphi(r,\varphi,t)\\ P(r,\varphi,t)\end{Bmatrix}=\begin{Bmatrix} \left[V_{x,i}(t)h_1(s)+V_{x,j}(t)h_2(s)\right]\cos\varphi+\left[V_{y,i}(t)h_1(s)+V_{y,j}(t)h_2(s)\right]\sin\varphi\\ -\left[V_{x,i}(t)h_1(s)+V_{x,j}(t)h_2(s)\right]\sin\varphi+\left[V_{y,i}(t)h_1(s)+V_{y,j}(t)h_2(s)\right]\cos\varphi\\ P_i(t)h_1(s)+P_j(t)h_2(s)\end{Bmatrix}\times\frac{r-a}{r_{\text{out}}-a}$$

$$+\sum_{n\geq1}\begin{Bmatrix} A_{1n}(t)h_{3n}(s)\cos\varphi+A_{2n}(t)h_{3n}(s)\sin\varphi\\ -A_{1n}(t)h_{3n}(s)\sin\varphi+A_{2n}(t)h_{3n}(s)\cos\varphi\\ A_{3n}(t)h_{3n}(s)\end{Bmatrix}\frac{r-a}{r_{\text{out}}-a}$$

$$+\sum_{m\geq0}\sum_{q=1,2}\sum_{k\geq1}\begin{Bmatrix} B_{1mqk}(t)\sin[k\pi(r-a)/(r_{\text{out}}-a)]\\ B_{2mqk}(t)\cos[(2k-1)(\pi/2)(r-a)/(r_{\text{out}}-a)]\\ B_{3mqk}(t)\cos[(2k-1)(\pi/2)(r-a)/(r_{\text{out}}-a)]\end{Bmatrix}\Phi_{mq}(\varphi) \tag{7}$$

### 3.2.2 Discretization by the Galerkin Method

To derive ordinary differential equations for these time variables, we substitute Eq. (7) into the following variational weighted-residual forms of the Navier-Stokes equations and the condition of continuity for each cell:

$$\int_0^{2\pi}\int_a^{r_{\text{out}}(\varphi)}\left[\rho\left(\frac{\partial V_r}{\partial t}+V_r\frac{\partial V_r}{\partial r}+V_\varphi\frac{1}{r}\frac{\partial V_r}{\partial\varphi}-\frac{V_\varphi^2}{r}\right)+\frac{\partial P}{\partial r}-\mu\left(\frac{\partial^2V_r}{\partial r^2}+\frac{1}{r}\frac{\partial V_r}{\partial r}+\frac{1}{r^2}\frac{\partial^2V_r}{\partial\varphi^2}-\frac{V_r}{r^2}-\frac{2}{r^2}\frac{\partial V_\varphi}{\partial\varphi}\right)\right]\delta V_r\,rdrd\varphi=0 \tag{8}$$

$$\int_0^{2\pi}\int_a^{r_{\text{out}}(\varphi)}\left[\rho\left(\frac{\partial V_\varphi}{\partial t}+V_r\frac{\partial V_\varphi}{\partial r}+V_\varphi\frac{1}{r}\frac{\partial V_\varphi}{\partial\varphi}+\frac{V_rV_\varphi}{r}\right)+\frac{1}{r}\frac{\partial P}{\partial\varphi}-\mu\left(\frac{\partial^2V_\varphi}{\partial r^2}+\frac{1}{r}\frac{\partial V_\varphi}{\partial r}+\frac{1}{r^2}\frac{\partial^2V_\varphi}{\partial\varphi^2}+\frac{2}{r^2}\frac{\partial V_r}{\partial\varphi}-\frac{V_\varphi}{r^2}\right)\right]$$

$$\times\delta V_\varphi\,rdrd\varphi=0 \tag{9}$$

$$\int_0^{2\pi}\int_a^{r_{\text{out}}(\varphi)}\frac{1}{K}\left[\frac{\partial P}{\partial t}+\left(C\frac{\partial}{\partial t}+K\right)\left(\frac{\partial V_r}{\partial r}+\frac{V_r}{r}+\frac{1}{r}\frac{\partial V_\varphi}{\partial\varphi}\right)\right]\delta P\cdot rdrd\varphi=S \tag{10}$$

where $S$ is the source term. For the rotated triangular array (Fig. 1(b)), $S$ is given by $\int_{\varphi_1}^{\varphi_2}V_{\text{src}}N_X\delta P\big|_{r=r_{\text{out}}}(ds/d\varphi)\times d\varphi$, where $N_X$ is the $X$-component of the inner unit normal vector on the outer circumstance of the cell; and $(\varphi_1,\varphi_2)$ is ($\pi/2$, $7\pi/6$), ($5\pi/6$, $7\pi/6$), and ($5\pi/6$, $3\pi/2$) for lower, mid, and upper regular hexagon cells along the inlet, respectively, and is (-$\pi/6$,$7\pi/2$), (-$\pi/6$, $\pi/6$), and (-$\pi/2$, $\pi/6$) for lower, mid, and upper regular hexagon cells along outlet, respectively. Substituting Eq. (7) into Eqs. (8)-(10) and synthesizing the equations for the cells, we obtain

[DOI: 10.1299/mej.14-00377]

the required ordinary differential equations in the following matrix form:

$$\mathbf{P}_0\dot{\mathbf{X}}_0 + \mathbf{Q}_0\mathbf{X}_0 + \mathbf{G} + \mathbf{R}_0 V_{\mathrm{src}} = \mathbf{0} \tag{11}$$

where $\mathbf{X}_0$ is the collection of the flow velocity components and pressure at the apexes, the generalized coordinates $A_{1n}$ - $A_{3n}$ for all cell sides, and the generalized coordinates $B_{1mqk}$ - $B_{3mqk}$ for all cells. The need of synthesizing arises from the fact that the equations for each cell are coupled through the flow velocity and pressure on the cell boundaries, over which the unknowns for adjacent cells coincide. Explanations for the derivation of Eq. (11) are given in Appendix A. The solution in stationary phase to Eq. (11) reveals the basic flow.

Let us consider the spatial periodicity for efficient analysis of the tube array system. Because there are many tubes in real situations, the basic flow is the same for each cell except near the inlet and outlet.

For the square array (Fig. 1(a)), the flow is not individually distinguishable for arbitrary lines $lT \le Y \le (l+1)T$. Based on this spatial periodicity, the basic flow analysis is conducted for one line represented by $0 \le X \le 3T$, $0 \le Y \le T$ under the boundary conditions $V_Y\big|_{Y=0} = V_Y\big|_{Y=T} = 0$, and the flow solution in the mid domain $T \le X \le 2T$, $0 \le Y \le T$ is applied to all cells in the vibration analysis conducted in Sec. 3.3. $V_{\mathrm{src}}$ is related to the velocity $V_{\mathrm{c}}$ at the tube clearances by $V_{\mathrm{src}} = (T-d)V_{\mathrm{c}}/T$, which can be obtained by considering the volume flow rate at each clearance the same based on the spatial periodicity and using the continuity condition $V_{\mathrm{c}}(T-d) = V_{\mathrm{src}}T$.

For the rotated triangular tube array (Fig. 1(b)), such a reduced-order model considering one line cannot be applied because the boundaries between adjacent lines (cell sides with gradient $dY/dX = \pm 1/\sqrt{3}$) are not streamlined. To solve this problem, the fluid domain bordered by thick solid lines shown in Fig. 3 is used as a reduced-order model, where positive and negative sources with magnitude $V_c$ are given at boundaries A and B. However, the analytical method explained above cannot readily be applied to this reduced-order model because the method basically assumes that:

(1) In Eq. (2), points $i$ and $j$ are apexes of the cells.
(2) In Eq. (5), the interval of $\varphi$ is $0 \le \varphi < 2\pi$ for all cells and $\Phi_{mq}$ is the same for $V_r$, $V_\varphi$, and $P$.

To eliminate these limitations, the author extended the theory and tool to allow for the following points:

(1) In Eq. (2), points $i$ and $j$ can be set at arbitrary places on the sides of the cells.
(2) In Eq. (5), the interval of $\varphi$ need not be the same for all cells and $\Phi_{mq}$ can be defined differently for $V_r$, $V_\varphi$, and $P$. For tube C in Fig. 3, for example, we define the interval of $\varphi$ as $0 \le \varphi \le \pi$ ($\varphi_{\min} = 0$, $\varphi_{\max} = \pi$), and alter Eq. (5) to

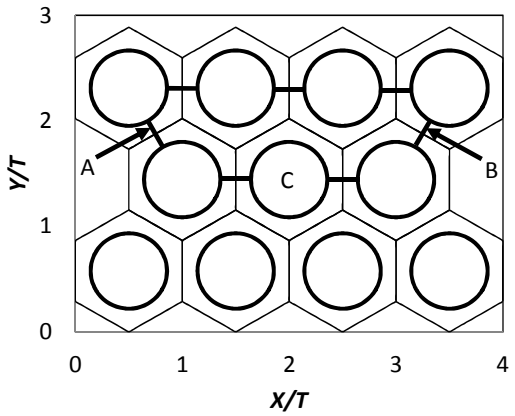


Fig. 3 Reduced domain for basic flow analysis in case of a rotated triangular tube array

$$\begin{Bmatrix} V_r(r,\varphi,t) \\ V_\varphi(r,\varphi,t) \\ P(r,\varphi,t) \end{Bmatrix} = \begin{Bmatrix} V_{r,\mathrm{out}}(\varphi,t) \\ V_{\varphi,\mathrm{out}}(\varphi,t) \\ P_{\mathrm{out}}(\varphi,t) \end{Bmatrix} \frac{r-a}{r_{\mathrm{out}}-a} + \sum_{\bar{m}\ge 1}\sum_{k\ge 1} \begin{Bmatrix} \overline{B}_{1\bar{m}k}(t)\overline{\Phi}_{1\bar{m}}(\varphi)\sin[k\pi(r-a)/(r_{\mathrm{out}}-a)] \\ \overline{B}_{2\bar{m}k}(t)\overline{\Phi}_{2\bar{m}}(\varphi)\cos[(2k-1)(\pi/2)(r-a)/(r_{\mathrm{out}}-a)] \\ \overline{B}_{3\bar{m}k}(t)\overline{\Phi}_{3\bar{m}}(\varphi)\cos[(2k-1)(\pi/2)(r-a)/(r_{\mathrm{out}}-a)] \end{Bmatrix} \tag{12}$$

with

[DOI: 10.1299/mej.14-00377]

$$\begin{Bmatrix} \overline{\Phi}_{1\overline{m}}(\varphi) \\ \overline{\Phi}_{2\overline{m}}(\varphi) \\ \overline{\Phi}_{3\overline{m}}(\varphi) \end{Bmatrix} = \begin{Bmatrix} \cos[(\overline{m}-1)\pi(\varphi-\varphi_{\min})/(\varphi_{\max}-\varphi_{\min})] \\ \sin[\overline{m}\,\pi(\varphi-\varphi_{\min})/(\varphi_{\max}-\varphi_{\min})] \\ \cos[(\overline{m}-1)\pi(\varphi-\varphi_{\min})/(\varphi_{\max}-\varphi_{\min})] \end{Bmatrix} \tag{13}$$

We note that because $(\varphi_{\min},\varphi_{\max}) \neq (0,2\pi)$, the bases given by Eq. (13) rather than $\Phi_{mq}(\varphi)$ defined by Eq. (6) should be used. Equation (2) remains applicable by defining line $ij$ as the cell side that corresponds to $0 \le \varphi \le \pi/6$, $\pi/6 \le \varphi \le \pi/2$, $\pi/2 \le \varphi \le 5\pi/6$, or $5\pi/6 \le \varphi \le \pi$. The flow analysis is conducted by thus developed reduced-order model. The cell flow for tube C is used as the flow around all the tubes in the dynamic analysis in Sec. 3.3, based on the fact that the basic flows in any cells are not individually distinguishable except near the inlet and outlet and have symmetry about lines $\varphi = 0$ and $\varphi = \pi$.

In this study, the stationary solution for the basic flow is obtained by introducing artificial inertia through the alteration of ($\partial V_r/\partial t$, $\partial V_\varphi/\partial t$) in Eqs. (8) and (9) to ($\beta\partial V_r/\partial t$, $\beta\partial V_\varphi/\partial t$), where $\beta$ is a positive constant. By this method, stability of the solution is improved and the stationary solution can be obtained approximately without changing the basic equations based on the fact that the non-stationary time-derivative terms damp in the stationary phase. The widely used method to improve stability is to introduce artificial viscous damping, which changes the basic equations. The present method may therefore serve as an alternative approximate method to analyze stationary flow also in other engineering problems.

### 3.3 Stability Analysis

In this section, the critical flow velocity above which fluid-elastic instability occurs is determined.

#### 3.3.1 Expression of Solution by Base Expansion

Let us express the fluid velocity components and pressure as

$$\overline{V}_r = V_r + v_r, \quad \overline{V}_\varphi = V_\varphi + v_\varphi, \quad \overline{P} = P + p \tag{14}$$

and conduct similar analysis for the vibrational components $v_r$, $v_\varphi$, and $p$. The vibrational fluid velocities in the $x$ and $y$ directions and the vibrational pressure on side $ij$ (outer circumference of the cell) are expressed by linear interpolation and base expansion:

$$\begin{Bmatrix} v_{x,\mathrm{out}}(\varphi,t) \\ v_{y,\mathrm{out}}(\varphi,t) \\ p_{\mathrm{out}}(\varphi,t) \end{Bmatrix} = \begin{Bmatrix} v_{x,i}(t) \\ v_{y,i}(t) \\ p_i(t) \end{Bmatrix} h_1(s) + \begin{Bmatrix} v_{x,j}(t) \\ v_{y,j}(t) \\ p_j(t) \end{Bmatrix} h_2(s) + \sum_{n\ge 1} \begin{Bmatrix} a_{1n}(t) \\ a_{2n}(t) \\ a_{3n}(t) \end{Bmatrix} h_{3n}(s) \tag{15}$$

By calculating $v_{r,\mathrm{out}}$ and $v_{\varphi,\mathrm{out}}$ from $v_{x,\mathrm{out}}$ and $v_{y,\mathrm{out}}$, the vibrational fluid velocity and pressure in arbitrary positions $(r,\varphi)$ are expressed as

$$\begin{Bmatrix} v_r(r,\varphi,t) \\ v_\varphi(r,\varphi,t) \\ p(r,\varphi,t) \end{Bmatrix} = \begin{Bmatrix} v_{r,\mathrm{out}}(\varphi,t) \\ v_{\varphi,\mathrm{out}}(\varphi,t) \\ p_{\mathrm{out}}(\varphi,t) \end{Bmatrix} \frac{r-a}{r_{\mathrm{out}}-a} + \sum_{m\ge 0}\sum_{q=1,2}\sum_{k\ge 1} \begin{Bmatrix} b_{1mqk}(t)\sin[k\pi(r-a)/(r_{\mathrm{out}}-a)] \\ b_{2mqk}(t)\cos[(2k-1)(\pi/2)(r-a)/(r_{\mathrm{out}}-a)] \\ b_{3mqk}(t)\cos[(2k-1)(\pi/2)(r-a)/(r_{\mathrm{out}}-a)] \end{Bmatrix} \Phi_{mq}(\varphi) \tag{16}$$

The first term on the right-hand side of Eq. (16) vanishes at the inner circumference $r = a$ and reduces to the solution [Eq. (15)] at the outer circumference $r = r_{\mathrm{out}}$. Therefore, the added base expansion term is given such that it vanishes at $r = r_{\mathrm{out}}$ and that the velocity component normal to the tube surface vanishes, i.e. $v_r|_{r=a} = 0$. By expressing $v_{r,\mathrm{out}}$ and $v_{\varphi,\mathrm{out}}$ in Eq. (16) in terms of $v_{x,\mathrm{out}}$ and $v_{y,\mathrm{out}}$ and substituting Eq. (15), we can express the vibrational components of the fluid velocity and pressure in arbitrary positions in terms of the vibrational components at the apexes and the generalized coordinates $a_{1n}$ - $a_{3n}$ and $b_{1mqk}$ - $b_{3mqk}$:

$$\begin{Bmatrix} v_r(r,\varphi,t) \\ v_\varphi(r,\varphi,t) \\ p(r,\varphi,t) \end{Bmatrix} = \begin{Bmatrix} \left[v_{x,i}(t)h_1(s)+v_{x,j}(t)h_2(s)\right]\cos\varphi + \left[v_{y,i}(t)h_1(s)+v_{y,j}(t)h_2(s)\right]\sin\varphi \\ -\left[v_{x,i}(t)h_1(s)+v_{x,j}(t)h_2(s)\right]\sin\varphi + \left[v_{y,i}(t)h_1(s)+v_{y,j}(t)h_2(s)\right]\cos\varphi \\ p_i(t)h_1(s)+p_j(t)h_2(s) \end{Bmatrix} \times \frac{r-a}{r_{\mathrm{out}}-a}$$

[DOI: 10.1299/mej.14-00377]

$$+\sum_{n\geq 1}\begin{Bmatrix} a_{1n}(t)h_{3n}(s)\cos\varphi + a_{2n}(t)h_{3n}(s)\sin\varphi \\ -a_{1n}(t)h_{3n}(s)\sin\varphi + a_{2n}(t)h_{3n}(s)\cos\varphi \\ a_{3n}(t)h_{3n}(s)\end{Bmatrix}\frac{r-a}{r_{\text{out}}-a}$$

$$+\sum_{m\geq 0}\sum_{q=1,2}\sum_{k\geq 1}\begin{Bmatrix} b_{1mqk}(t)\sin[k\pi(r-a)/(r_{\text{out}}-a)] \\ b_{2mqk}(t)\cos[(2k-1)(\pi/2)(r-a)/(r_{\text{out}}-a)] \\ b_{3mqk}(t)\cos[(2k-1)(\pi/2)(r-a)/(r_{\text{out}}-a)]\end{Bmatrix}\Phi_{mq}(\varphi) \tag{17}$$

### 3.3.2 Discretization by the Galerkin Method

Altering $V_r$, $V_\varphi$, $P$ in Eqs. (8) and (9) to $\overline{V}_r$, $\overline{V}_\varphi$, and $\overline{P}$ gives the equations of motion satisfied by $\overline{V}_r$, $\overline{V}_\varphi$, and $\overline{P}$. By substituting Eq. (14) into these equations, making the linear approximation for the vibrational components, and using the equations that are satisfied by the basic flow, we obtain the following equations of motion for each cell:

$$\int_0^{2\pi}\int_a^{r_{\text{out}}(\varphi)}\left\{\rho\left[\frac{\partial v_r}{\partial t}+V_r\frac{\partial v_r}{\partial r}+v_r\frac{\partial V_r}{\partial r}+\frac{1}{r}\left(V_\varphi\frac{\partial v_r}{\partial\varphi}+v_\varphi\frac{\partial V_r}{\partial\varphi}\right)-\frac{1}{r}(V_\varphi v_\varphi+v_\varphi V_\varphi)\right]\right.$$
$$\left.+\frac{\partial p}{\partial r}-\mu\left(\nabla^2 v_r-\frac{v_r}{r^2}-\frac{2}{r^2}\frac{\partial v_\varphi}{\partial\varphi}\right)\right\}\delta v_r r dr d\varphi = 0 \tag{18}$$

$$\int_0^{2\pi}\int_a^{r_{\text{out}}(\varphi)}\left\{\rho\left[\frac{\partial v_\varphi}{\partial t}+V_r\frac{\partial v_\varphi}{\partial r}+v_r\frac{\partial V_\varphi}{\partial r}+\frac{1}{r}\left(V_\varphi\frac{\partial v_\varphi}{\partial\varphi}+v_\varphi\frac{\partial V_\varphi}{\partial\varphi}\right)+\frac{1}{r}(V_r v_\varphi+v_r V_\varphi)\right]\right.$$
$$\left.+\frac{1}{r}\frac{\partial p}{\partial\varphi}-\mu\left(\nabla^2 v_\varphi+\frac{2}{r^2}\frac{\partial v_r}{\partial\varphi}-\frac{v_\varphi}{r^2}\right)\right\}\delta v_\varphi r dr d\varphi = 0 \tag{19}$$

Applying similar procedures to Eq. (10) and considering the tube velocity in the outer normal direction of the tube as a source, we obtain

$$\int_0^{2\pi}\int_a^{r_{\text{out}}(\varphi)}\frac{1}{K}\left[\frac{\partial p}{\partial t}+\left(C\frac{\partial}{\partial t}+K\right)\left(\frac{\partial v_r}{\partial r}+\frac{v_r}{r}+\frac{1}{r}\frac{\partial v_\varphi}{\partial\varphi}\right)\right]\delta p\cdot r dr d\varphi-\int_0^{2\pi}(\dot{q}_x\cos\varphi+\dot{q}_y\sin\varphi)\delta p\big|_{r=a}a d\varphi=0 \tag{20}$$

The equations of motion of each tube are given by

$$\begin{Bmatrix} m_b(\ddot{q}_x+2\zeta_b\omega_x\dot{q}_x+\omega_x^2 q_x) \\ m_b(\ddot{q}_y+2\zeta_b\omega_y\dot{q}_y+\omega_y^2 q_y)\end{Bmatrix}+\int_0^{2\pi}\begin{Bmatrix} p|_{r=a}\cos\varphi+F_{\text{vis}}\sin\varphi \\ p|_{r=a}\sin\varphi-F_{\text{vis}}\cos\varphi\end{Bmatrix}a d\varphi=0 \tag{21}$$

where the viscous force $F_{\text{vis}}$ is calculated by the procedure explained in Appendix B. The positions of cells are fixed during the tube motions.

By substituting Eq. (17) into Eqs. (18)-(21) and synthesizing the equations for the cells, we obtain ordinary differential equations for the vibrational components of the fluid velocity and pressure at the apexes and the generalized coordinates. These equations can be expressed in the form of a matrix equation:

$$\mathbf{P}_1\dot{\mathbf{X}}_1+\mathbf{Q}_1\mathbf{X}_1=\mathbf{0} \tag{22}$$

where $\mathbf{X}_1$ is the collection of the vibrational fluid velocity and pressure at the apexes, the generalized coordinates $a_{1n}$ - $a_{3n}$ for all cell sides, the generalized coordinates $b_{1mqk}$ - $b_{3mqk}$ for all cells, and the displacements and velocities of all tubes. The need of synthesizing arises from the fact that the equations for each cell are coupled through the fluid velocity and pressure on the cell boundaries, over which the fluid unknowns for adjacent cells coincide. Explanations for the derivation of Eq. (22) are given in Appendix C. If the real parts of the eigenvalues of the matrix $-\mathbf{P}_1^{-1}\mathbf{Q}_1$ are smaller than zero, the system is stable.

Let us define the following dimensionless quantities.

$$(\hat{r},\hat{r}_{\text{out}})=(r,r_{\text{out}})/a,\quad \hat{t}=\omega_x t,\quad (\hat{v}_r,\hat{v}_\varphi)=(v_r,v_\varphi)/a\omega_x,$$
$$(\hat{V}_r,\hat{V}_\varphi)=(V_r,V_\varphi)/V_c,\quad (\hat{q}_x,\hat{q}_y)=(q_x,q_y)/a,\quad \hat{p}=p/\rho a^2\omega_x^2,$$

[DOI: 10.1299/mej.14-00377]

$$\hat{F}_{\mathrm{vis}} = F_{\mathrm{vis}} / \mu\omega_x, \quad \hat{K} = K / \rho a^2 \omega_x^2, \quad \hat{C} = C / \rho a^2 \omega_x \tag{23}$$

The basic and vibrational components of the fluid velocity are normalized by $V_c$ and $a\omega_x$, respectively. Using these dimensionless quantities, Eqs. (18)-(21) can be transformed into

$$\int_0^{2\pi}\int_1^{\hat{r}_{\mathrm{out}}(\varphi)} \left\{ \frac{\partial \hat{v}_r}{\partial \hat{t}} + \underline{\frac{V_c}{a\omega_x}} \left[ \hat{V}_r \frac{\partial \hat{v}_r}{\partial \hat{r}} + \hat{v}_r \frac{\partial \hat{V}_r}{\partial \hat{r}} + \frac{1}{\hat{r}} \left( \hat{V}_\varphi \frac{\partial \hat{v}_r}{\partial \varphi} + \hat{v}_\varphi \frac{\partial \hat{V}_r}{\partial \varphi} \right) - \frac{1}{\hat{r}} (\hat{V}_\varphi \hat{v}_\varphi + \hat{v}_\varphi \hat{V}_\varphi) \right] \right.$$

$$\left. + \frac{\partial \hat{p}}{\partial \hat{r}} - \frac{\mu}{\rho a^2 \omega_x} \left( \hat{\nabla}^2 \hat{v}_r - \frac{\hat{v}_r}{\hat{r}^2} - \frac{2}{\hat{r}^2} \frac{\partial \hat{v}_\varphi}{\partial \varphi} \right) \right\} \delta\hat{v}_r \cdot \hat{r} d\hat{r} d\varphi = 0 \tag{24}$$

$$\int_0^{2\pi}\int_1^{\hat{r}_{\mathrm{out}}(\varphi)} \left\{ \frac{\partial \hat{v}_\varphi}{\partial t} + \underline{\frac{V_c}{a\omega_x}} \left[ \hat{V}_r \frac{\partial \hat{v}_\varphi}{\partial \hat{r}} + \hat{v}_r \frac{\partial \hat{V}_\varphi}{\partial \hat{r}} + \frac{1}{\hat{r}} \left( \hat{V}_\varphi \frac{\partial \hat{v}_\varphi}{\partial \varphi} + \hat{v}_\varphi \frac{\partial \hat{V}_\varphi}{\partial \varphi} \right) + \frac{1}{\hat{r}} (\hat{V}_r \hat{v}_\varphi + \hat{v}_r \hat{V}_\varphi) \right] \right.$$

$$\left. + \frac{\partial \hat{p}}{\hat{r}\partial \varphi} - \frac{\mu}{\rho a^2 \omega_x} \left( \nabla^2 \hat{v}_\varphi + \frac{2}{\hat{r}^2} \frac{\partial \hat{v}_r}{\partial \varphi} - \frac{\hat{v}_\varphi}{\hat{r}^2} \right) \right\} \delta\hat{v}_\varphi \cdot \hat{r} d\hat{r} d\varphi = 0 \tag{25}$$

$$\int_0^{2\pi}\int_1^{\hat{r}_{\mathrm{out}}(\varphi)} \left[ \frac{1}{\hat{K}} \frac{\partial \hat{p}}{\partial \hat{t}} + \left( \frac{\hat{C}}{\hat{K}} \frac{\partial}{\partial \hat{t}} + 1 \right) \left( \frac{\partial \hat{v}_r}{\partial \hat{r}} + \frac{\hat{v}_r}{\hat{r}} + \frac{\partial \hat{v}_\varphi}{\hat{r}\partial \varphi} \right) \right] \delta\hat{p}\, \hat{r} d\hat{r} d\varphi - \int_0^{2\pi} \left( \frac{d\hat{q}_x}{d\hat{t}} \cos\varphi + \frac{d\hat{q}_y}{d\hat{t}} \sin\varphi \right) \delta\hat{p}\big|_{\hat{r}=1} d\varphi = 0 \tag{26}$$

$$\underline{\frac{m_b}{\rho a^2}} \begin{Bmatrix} \dfrac{d^2\hat{q}_x}{d\hat{t}^2} + 2\underline{\zeta_b} \dfrac{d\hat{q}_x}{d\hat{t}} + \hat{q}_x \\ \dfrac{d^2\hat{q}_y}{d\hat{t}^2} + 2\underline{\zeta_b} \underline{\dfrac{\omega_y}{\omega_x}} \dfrac{d\hat{q}_y}{d\hat{t}} + \underline{\dfrac{\omega_y^2}{\omega_x^2}} \hat{q}_y \end{Bmatrix} + \int_0^{2\pi} \hat{p}\big|_{\hat{r}=1} \begin{Bmatrix} \cos\varphi \\ \sin\varphi \end{Bmatrix} d\varphi + \frac{\mu}{\rho a^2 \omega_x} \int_0^{2\pi} \hat{F}_{\mathrm{vis}} \begin{Bmatrix} \sin\varphi \\ -\cos\varphi \end{Bmatrix} d\varphi = 0 \tag{27}$$

Due to the small compressibility and dynamic viscosity, the compressibility and viscous terms are small. Therefore, the underlined terms lead to the following dimensionless parameters of concern; the reduced velocity $V_{\mathrm{reduc}} = V_{\mathrm{c}} / (\omega_x d / 2\pi)$, mass parameter $m_b / \rho d^2$, mass-damping parameter $m_b 2\pi\zeta_b / \rho d^2$, and $\omega_y / \omega_x$.

Conventional case studies examine the relation between the critical reduced velocity, at which fluid-elastic instability occurs, and the mass-damping parameter by prescribing the other dimensionless parameters. The present analysis provides a theoretical foundation for the conventional case studies by using the fluid dynamics governing equations as above.

## 4. Numerical Results

### 4.1 Case of the Square Array

Figure 4 shows results for the basic flow determined by using the reduced-order model. The parameters are $T/d$ =1.33, $\Delta\hat{t}$ =0.0628, $\hat{t}_0$ =6000 $\Delta\hat{t}$, $\beta$ =40, and $Re$=300. The base functions with $n$ =1-2, $m$ =0-2, and $k$ =1 are considered. We see from Fig. 4(a) that the circumferential flow is large near the clearances. The cross-sectional mean of $\hat{V}_\varphi$ at $\varphi$ =270 deg shown in Fig. 4(b) represents the ratio of this mean velocity to its prescribed value. The condition that this ratio equals unity was difficult to satisfy due to the limitation of the method. The critical velocity was calculated from the eigenvalue problem for Eq. (22) using the basic flow. For this reason, the eigenvalue problem-based critical velocity was corrected by multiplying it by the ratio 0.8 shown in Fig. 4(b). Similar correction is made for the case of rotated triangular array in Sec. 4.2.

Figure 5 illustrates the critical reduced velocity for a square tube array shown in Fig. 1(a). The mass-damping parameter $m_b 2\pi\zeta_b / \rho d^2$ is increased by raising the damping ratio for a fixed mass parameter $m_b / \rho d^2$ =1.85. The base functions with $n$ =1-2, $m$ =1, and $k$ =1 are considered. For the sake of comparison, earlier experimental results (Tanaka et al., 2002) are shown by a black circle. The results obtained by the present analysis show acceptable agreement with the experimental data, verifying the proposed semi-analytical method. We can see from Fig. 5 that the critical reduced velocity rises with increasing mass-damping parameter.

[DOI: 10.1299/mej.14-00377]

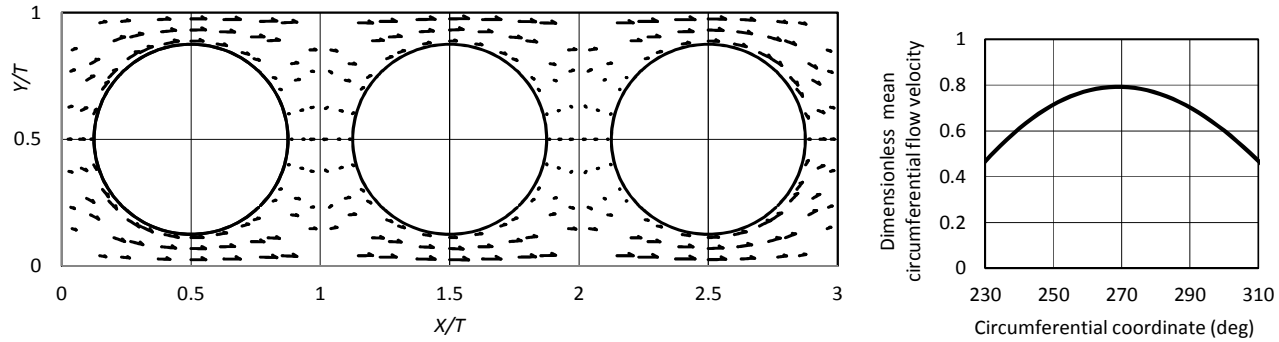


(a) (b)

Fig. 4 Results for the basic flow; (a) flow patern, (b) the mean of dimensionless $\hat{V}_{\varphi}$ over the cross-section $1 \le \hat{r} \le \hat{r}_{\text{out}}(\varphi)$ near the clearance $\varphi$=270 deg in the mid cell

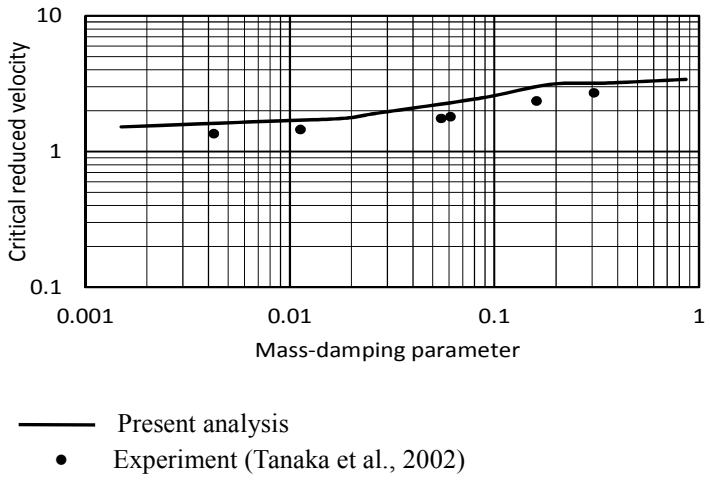


Fig. 5 Critical reduced velocity for the square tube array ($T/d$=1.33, $m_b/\rho d^2$=1.85, $\omega_y/\omega_x$=1, water flow)

### 4.2 Case of Rotated Triangular Array

Figure 6 shows the critical reduced velocity for a rotated triangular tube array shown in Fig. 1(b). The domain consisting of the eleven cells shown in Fig. 1(b) is considered. The mass-damping parameter $m_b 2\pi\zeta_b/\rho d^2$ is increased by raising the damping ratio for a fixed mass-parameter. The damping ratio $\zeta_b$ is 0.00111 when the mass-damping parameter is 1.3. The base functions with $n$=1-2, $m$=1, and $k$=1 are retained. For the sake of comparison, earlier experimental results (Weaver and Grover, 1978) are shown using black circles. The present analytical results show acceptable correlation to the experimental data, thus supporting the validity of the present semi-analytical method in the interval shown in the figure.

For a higher mass-damping parameter, e.g. 14, the critical reduced velocity 16.2 obtained by the present analysis is considerably larger than the experimental result 11.5, which is a limitation at the present stage and must be studied in future work. A motivation of this paper is that the interval shown Fig. 6 covers the range $2.2 \le m_b 2\pi\zeta_b/\rho d^2 \le 3.6$ which is referred to as a practically important condition in an experimental work (Mureithi et al., 2005).

The critical reduced velocity for a larger pitch-diameter ratio is shown in Fig. 7. The result for the previous case is shown by dotted line for the sake of comparison. We see that the critical reduced velocity is increased to some extent by raising the pitch-diameter ratio.

Figure 8 shows examples of the dependence of the damping ratio $\zeta_{\text{eig}}$ associated with the eigenvalue on the reduced velocity $V_{\text{reduc}}$ for the case of Fig. 6. Using Fig. 8, we not only confirm that $\zeta_{\text{eig}}$ is zero at the critical reduced velocity shown in Fig. 6, but also make the following check. When $m_b 2\pi\zeta_b/\rho d^2$=2.33 ($\zeta_b$=0.00201) and $V_{\text{reduc}}$=10, for example, $\zeta_{\text{eig}}$ equals $-0.002$. This means that by adding damping ratio 0.002 to double the mass-damping parameter, the system can be stabilized in $V_{\text{reduc}}$<10. That is, the critical reduced velocity can be increa-

[DOI: 10.1299/mej.14-00377]

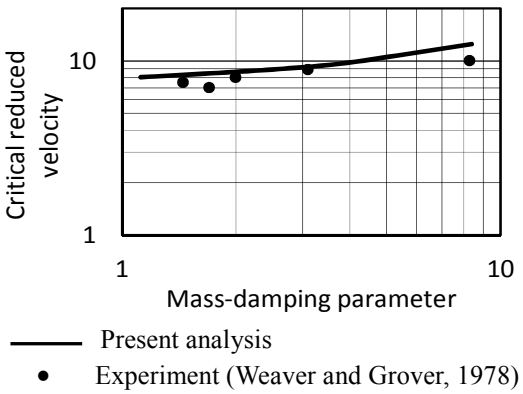


Fig. 6 Critical reduced velocity for the rotated triangular tube array ($T/d$=1.375, $m_b/\rho d^2$ =185, $\omega_y/\omega_x$=1, air flow)

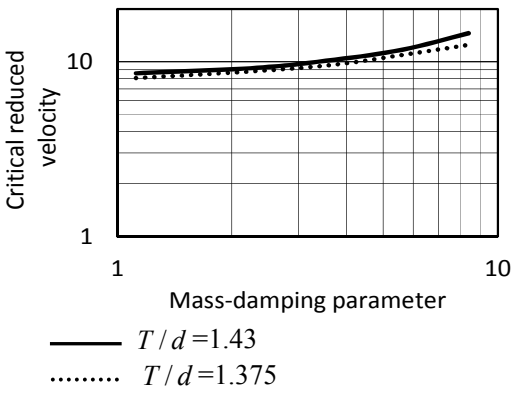


Fig. 7 Effect of the pitch-diameter ratio on critical reduced velocity for the rotated triangular tube array ($m_b/\rho d^2$=185, $\omega_y/\omega_x$=1, air flow)

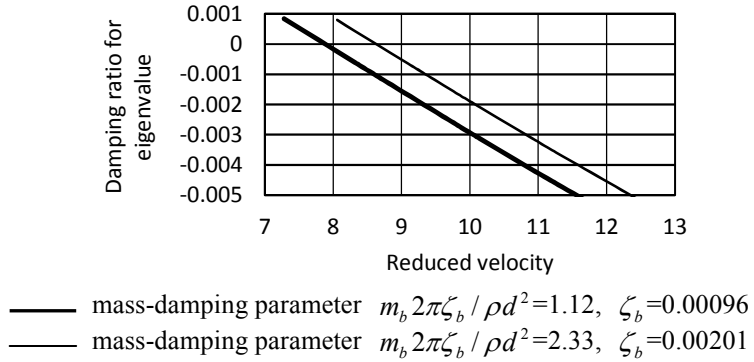


Fig. 8 Damping ratio associated with the eigenvalue

sed to 10. This predicted critical reduced velocity coincides with the result shown in Fig. 6.

Numerical results regarding instability in the flow direction mentioned at the end of the introduction are presented below.

Figure 9 shows the result for the case where the ratio of the tube eigenfrequency $\omega_y$ in the $y$ direction to that $\omega_x$ in the $x$ direction (flow direction) is raised by increasing $\omega_y$. We can see from Fig. 9 that the critical reduced velocity rises with increasing $\omega_y/\omega_x$ to reach a constant value. To examine the reason, unstable modes are shown in Fig. 10. Figure 10(a) shows the original case $\omega_y/\omega_x$=1 while Fig. 10(b) illustrates the case of $\omega_y/\omega_x$=1.9, above which the critical reduced velocity remains constant.

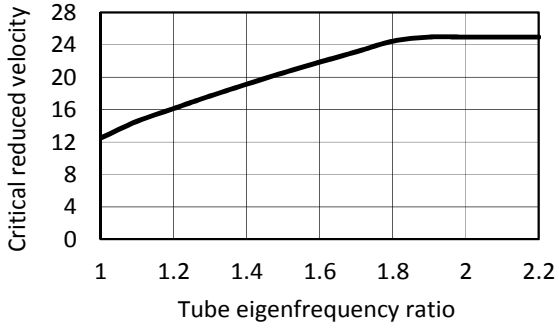


Fig. 9 Critical reduced velocity versus tube eigenfrequency ratio $\omega_y/\omega_x$
($\omega_y$ is increased, mass-damping parameter $m_b 2\pi\zeta_b/\rho d^2$=8.39, $\zeta_b$=0.00722)

[DOI: 10.1299/mej.14-00377]

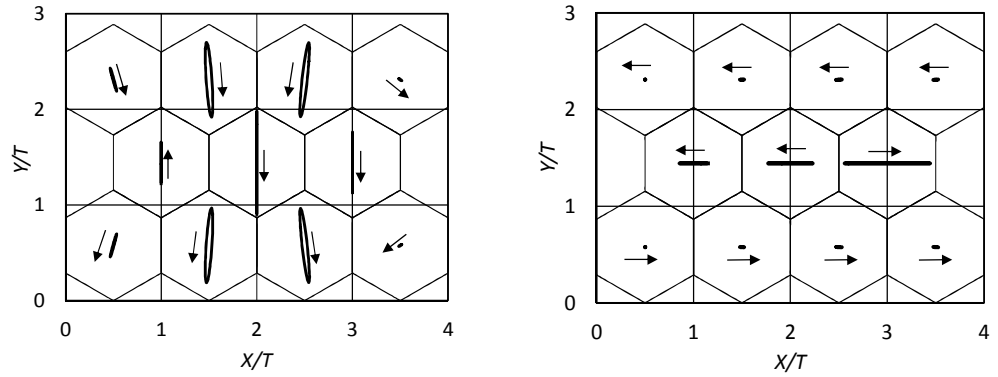


(a) $\omega_y/\omega_x$=1, $V_{\mathrm{reduc}}$=12.5 (b) $\omega_y/\omega_x$=1.9, $V_{\mathrm{reduc}}$=25

Fig. 10 Unstable modes in case of Fig. 9 at $\omega_y/\omega_x$=1 and 1.9

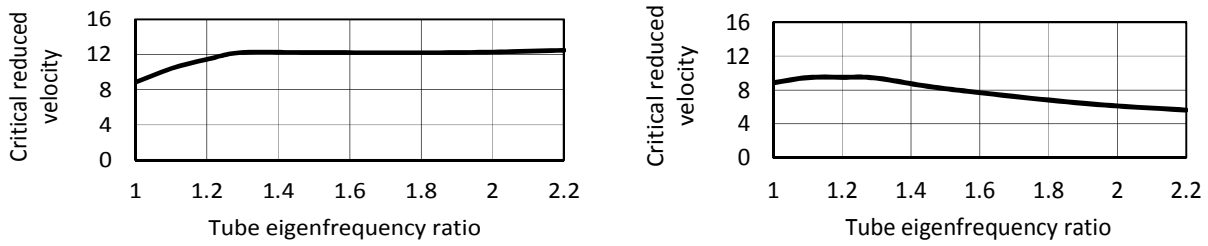


(a) $\omega_y$ is increased (b) $\omega_x$ is decreased

Fig. 11 Critical reduced velocity versus tube eigenfrequency ratio $\omega_y/\omega_x$
(mass-damping parameter $m_b 2\pi\zeta_b/\rho d^2$=2.33, $\zeta_b$=0.00201)

Instability is mainly in the $y$ direction when $\omega_y/\omega_x$=1 (Fig. 10(a)). Therefore, the increase in $\omega_y$ raises the critical reduced velocity. However, further increase in $\omega_y/\omega_x$ has a destabilizing effect on vibration in the $x$ direction with the lower eigenfrequency $\omega_x$, as can be seen from Fig. 10(b). Once the direction of instability changes from the $y$ direction to the $x$ direction, the increase in $\omega_y$ no longer boosts the critical reduced velocity. Therefore, the critical reduced velocity becomes constant with increasing $\omega_y/\omega_x$, as shown in Fig. 9. It should be noted that instability is mainly in the $y$-direction over the interval $1<\omega_y/\omega_x<1.9$ and that the direction of instability changes to the flow direction suddenly at $\omega_y/\omega_x$=1.9.

For smaller mass-damping parameters, stability decreases. Therefore, the stabilizing effect mentioned above is predicted to be restricted. That is, the following trends are predicted: (a) the increase in the critical reduced velocity achieved by the increase in $\omega_y/\omega_x$ decreases; and (b) the transition of the direction of instability from the $y$ direction to the $x$ direction, as indicated by the critical reduced velocity remaining unchanged despite increasing $\omega_y/\omega_x$, arises at smaller values of the critical reduced velocity and $\omega_y/\omega_x$. An example result confirming these predictions is shown in Fig. 11(a). By comparing Fig. 11(a) with Fig. 9, we confirm that the critical reduced velocity and $\omega_y/\omega_x$ at the transition are reduced from 25 to 12 and 1.9 to 1.3, respectively. The critical reduced velocity 12 for large $\omega_y/\omega_x$ correlates to the experimental result (Mureithi et al., 2005) obtained under similar conditions $T/d$ =1.37, $2.2<m_b 2\pi\zeta_b/\rho d^2<3.6$, and $\zeta_b$=0.3%-0.5%, however, more detailed comparison with experimental results is required.

For the conservative design, it is helpful to estimate the case where $\omega_y/\omega_x$ is raised not by increasing $\omega_y$ but by decreasing $\omega_x$. An example for this case is presented in Fig. 11(b) (in this figure, the reduced velocity is defined as $V_{\mathrm{reduc},y}=V_{\mathrm{c}}/(\omega_y d/2\pi)$ by normalizing using $\omega_y$ because $\omega_x$ is changed). Within the interval $1<\omega_y/\omega_x<1.3$, the decrease in $\omega_x$ has almost no influence on the critical reduced velocity, meaning that instability is in the $y$ direction. However, further decrease in $\omega_x$ triggers a transition in the direction of instability to the $x$ direction and hence a decrease in critical reduced velocity.

The numerical study in Sec. 4 considers the viscous force calculated by the method explained in Appendix B.

[DOI: 10.1299/mej.14-00377]

Numerical calculation was conducted also for the case without the viscous force, and it was confirmed that the difference between the results with and without the viscous effect is very small.

## 5. Conclusions

The critical reduced velocity for the threshold of fluid-elastic instability of a tube array subject to cross-flow was predicted using a newly developed semi-analytical method. The conclusions are summarized as follows:

(1) A semi-analytical method was developed by considering the system as a collection of regular polygon cells, expressing unknowns on each side of the cells by base expansion, and deriving the polar coordinate expressions of the solutions in each cell allowing for circumferential variation in the interval of the radial coordinate.
(2) The method was verified by comparing with earlier experimental results.
(3) Instability in the flow direction induced in a rotated triangular tube array with different eigenfrequencies in the transverse and flow directions was predicted by the present semi-analytical method.

### Appendix A: Explanations for the Derivation of Eq. (11)

Derivation of Eq. (11) through the substitution of Eq. (7) into Eqs. (8)-(10) requires very lengthy hand calculation, especially for the many nonlinear terms $V_r(\partial V_\varphi / \partial r)\delta V_\varphi$ etc. Each of them consists of three factors that have many terms, as can be seen from Eq. (7). To overcome this difficulty, we first express Eq. (7) as

$$\begin{Bmatrix} V_r(r,\varphi,t) \\ V_\varphi(r,\varphi,t) \\ P(r,\varphi,t) \end{Bmatrix} = \sum_{I\geq 1} \begin{Bmatrix} C_{1I}(t)F_{1I}(r,\varphi) \\ C_{2I}(t)F_{2I}(r,\varphi) \\ C_{3I}(t)F_{3I}(r,\varphi) \end{Bmatrix} \tag{A1}$$

by defining the index number $I$ of each term and letting $C_{1I}$-$C_{3I}$ and $F_{1I}$-$F_{3I}$ be the $I$ th time variable and spatial term, respectively. It is necessary to obtain the expression (A1) for each $\varphi$-interval that corresponds to one cell side, because Eq. (7) contains the time variables defined for one cell side. We then assign the index number $N_{1J}$-$N_{3J}$ to the components $C_{1J}$-$C_{3J}$ of $\mathbf{X}_0$ in Eq. (11). By using Eq. (A1), the nonlinear term $V_r(\partial V_\varphi / \partial r)\delta V_\varphi$, for example, can be calculated as

$$\int_0^{2\pi}\int_a^{r_{\text{out}}(\varphi)} \rho V_r \frac{\partial V_\varphi}{\partial r}\delta V_\varphi r dr d\varphi = \sum_{I\geq 1}\delta C_{2I} \sum_{I_1\geq 1}\sum_{I_2\geq 1} C_{1I_1}C_{2I_2}\rho \int_0^{2\pi}\int_a^{r_{\text{out}}(\varphi)} F_{1I_1}\frac{\partial F_{2I_2}}{\partial r}F_{2I} r dr d\varphi \tag{A2}$$

whose coefficient of $\delta C_{2I}$ contributes to the $N_{2I}$ th component of $\mathbf{G}$ in Eq. (11). By repeating similar procedure, the nonlinear term of Eq. (11) can be determined.

The linear term $(\partial V_\varphi / \partial t)\delta V_\varphi$, for example, becomes

$$\int_0^{2\pi}\int_a^{r_{\text{out}}(\varphi)} \rho(\partial V_\varphi / \partial t)\delta V_\varphi r dr d\varphi = \sum_{I\geq 1}\delta C_{2I}\sum_{I_1\geq 1}\dot{C}_{2I_1}\rho\int_0^{2\pi}\int_a^{r_{\text{out}}(\varphi)} F_{2I_1}F_{2I} r dr d\varphi \tag{A3}$$

whose coefficient of $\delta C_{2I}\dot{C}_{2I_1}$ contributes to the $(N_{2I}, N_{2I_1})$ component of $\mathbf{P}_0$ in Eq. (11).

### Appendix B: Method of Examining the Influence of Viscous Force on Critical Reduced Velocity

In this problem, both the pressure gradient in the main flow and the motion of the boundary are present, and terms that explicitly contain the imaginary unit must be evaluated in the time domain. For these reasons, the full derivation is presented. Given the minute thickness of the boundary layer compared to the tube radius, the curvature of the boundary layer is not considered. The equation of motion for the main flow just outside the boundary layer is

$$\partial v_\varphi^{(m)} / \partial t = (-1/\rho)\partial p^{(m)} / a\partial\varphi \tag{B1}$$

Defining the amplitude functions $\tilde{v}_\varphi^{(m)}$ and $\tilde{p}^{(m)}$ gives

$$\mathrm{i}\omega\tilde{v}_\varphi^{(m)} = (-1/\rho)\partial\tilde{p}^{(m)} / a\partial\varphi \tag{B2}$$

For the boundary layer flow, the flow velocity in the $r$ direction is very small. Therefore, the equation of motion

[DOI: 10.1299/mej.14-00377]

in the $r$ direction reduces to $\partial p_{BL}/\partial r = 0$. Hence, the condition $p_{BL}\big|_{r\to\infty} = p^{(m)}(\varphi,t)$ requires $p_{BL}(r,\varphi,t) = p^{(m)}(\varphi,t)$. Because the boundary layer is very thin, an approximation $\nabla^2 v_{\varphi,BL} \cong \partial^2 v_{\varphi,BL}/\partial r^2$ holds. We thus obtain

$$\partial v_{\varphi,BL}/\partial t = (-1/\rho)\partial p^{(m)}/a\partial\varphi + \nu\partial^2 v_{\varphi,BL}/\partial r^2 \tag{B3}$$

We solve Eq. (B3) under the boundary conditions:

$$v_{\varphi,BL}(r,\varphi,t)\big|_{r\to\infty} = \tilde{v}_\varphi^{(m)}(\varphi)\mathrm{e}^{\mathrm{i}\omega t},\quad v_{\varphi,BL}(r,\varphi,t)\big|_{r=a} = \tilde{v}_\varphi^{(b)}(\varphi)\mathrm{e}^{\mathrm{i}\omega t} \tag{B4}$$

Expressing the solution as

$$v_{\varphi,BL}(r,\varphi,t) = \tilde{v}_{\varphi,BL}(r,\varphi)\mathrm{e}^{\mathrm{i}\omega t} \tag{B5}$$

and using Eq. (B2), we obtain

$$\partial^2\tilde{v}_{\varphi,BL}/\partial r^2 - (\mathrm{i}\omega/\nu)\tilde{v}_{\varphi,BL}(r,\varphi) = -(\mathrm{i}\omega/\nu)\,\tilde{v}_\varphi^{(m)}(\varphi) \tag{B6}$$

$$\tilde{v}_{\varphi,BL}(r,\varphi)\big|_{r\to\infty} = \tilde{v}_\varphi^{(m)}(\varphi),\qquad \tilde{v}_{\varphi,BL}(r,\varphi)\big|_{r=a} = \tilde{v}_\varphi^{(b)}(\varphi) \tag{B7}$$

The characteristic root $\alpha$ of the homogeneous equation associated with Eq. (B6) satisfies $\alpha^2 = \mathrm{i}\omega/\nu$, which admits $\alpha = -(1+\mathrm{i})(\omega/2\nu)^{1/2}$ for the bounded solution. Hence, the general solution to Eq. (B6) is then given by

$$\tilde{v}_{\varphi,BL}(r,\varphi) = F(\varphi)\exp[(-1-\mathrm{i})(\omega/2\nu)^{1/2}(r-a)] + \tilde{v}_\varphi^{(m)}(\varphi) \tag{B8}$$

Using Eq. (B7) to determine the arbitrary function $F(\varphi)$ yields

$$v_{\varphi,BL}(r,\varphi,t) = [v_\varphi^{(b)}(\varphi,t) - v_\varphi^{(m)}(\varphi,t)]\exp[(-1-\mathrm{i})(\omega/2\nu)^{1/2}(r-a)] + v_\varphi^{(m)}(\varphi,t) \tag{B9}$$

Because $v_\varphi^{(b)}(\varphi,t)$ and $v_\varphi^{(m)}(\varphi,t)$ are the velocities of the tube and main flow in the $\varphi$ direction at $r=a$, the viscous force can be estimated by

$$F_{\mathrm{vis}}(\varphi,t) = \mu\frac{\partial v_{\varphi,BL}}{\partial r}\bigg|_{r=a} = \underline{-\mu(1+\mathrm{i})\left(\frac{\omega}{2\nu}\right)^{1/2}}(-\dot{q}_x\sin\varphi + \dot{q}_y\cos\varphi - v_\varphi\big|_{r=a}) \tag{B10}$$

Equation (B10) explicitly contains i and cannot readily be calculated in the time-domain. For this reason, the present study examined the influence of viscous force on the critical reduced velocity by transforming the underlined term into $(\omega/2\nu)^{1/2} + \mathrm{i}\omega(2\nu\omega)^{-1/2}$ and regarding $\mathrm{i}\omega$ the time-derivative operator ($\omega$ in parentheses is approximated as the tube eigenfrequency because the $\omega$-dependence is weakened to 1/2 power). Numerical results thus obtained show that the influence can be neglected.

**Appendix C: Explanations for the Derivation of Eq. (22)**

For each $\varphi$-interval that corresponds to one cell side, we first express Eq. (17) as

$$\begin{Bmatrix} v_r(r,\varphi,t) \\ v_\varphi(r,\varphi,t) \\ p(r,\varphi,t) \end{Bmatrix} = \sum_{J\geq 1}\begin{Bmatrix} c_{1J}(t)f_{1J}(r,\varphi) \\ c_{2J}(t)f_{2J}(r,\varphi) \\ c_{3J}(t)f_{3J}(r,\varphi) \end{Bmatrix} \tag{C1}$$

by defining the index number $J$ of each term and letting $c_{1J}$-$c_{3J}$ and $f_{1J}$-$f_{3J}$ be the $J$th time variable and spatial term, respectively. We then assign index numbers $N'_{1J}$-$N'_{3J}$ to the components $c_{1J}$-$c_{3J}$ of $\mathbf{X}_1$ in Eq. (22). By using Eqs. (A1) and (C1), a term $v_r(\partial V_\varphi/\partial r)\delta v_\varphi$ in Eq. (19), for example, can be calculated as

$$\int_0^{2\pi}\int_a^{r_{\mathrm{out}}(\varphi)} \rho v_r\frac{\partial V_\varphi}{\partial r}\delta v_\varphi r dr d\varphi = \sum_{J\geq 1}\delta c_{2J}\sum_{J_1\geq 1} c_{1J_1}\left(\sum_{I\geq 1} C_{2I}\rho\int_0^{2\pi}\int_a^{r_{\mathrm{out}}(\varphi)} f_{1J_1}\frac{\partial F_{2I}}{\partial r}f_{2J}\,r dr d\varphi\right) \tag{C2}$$

whose coefficient of $\delta c_{2J}c_{1J_1}$ contributes to the $(N'_{2J}, N'_{1J_1})$ component of $\mathbf{Q}_1$ in Eq. (22). By repeating similar procedure, the matrices $\mathbf{P}_1$ and $\mathbf{Q}_1$ in Eq. (22) can be determined.

## References

Chen, S. S., Instability mechanisms and stability criteria of a group of circular cylinders subjected to cross-flow. Part I: Theory, ASME Journal of Vibration, Acoustics, Stress, and Reliability in Design, Vol. 105, Issue 1 (1983), pp. 51-58.

Chen, S. S., Instability mechanisms and stability criteria of a group of circular cylinders subjected to cross-flow. Part II:

[DOI: 10.1299/mej.14-00377]  

Numerical results and discussions, ASME Journal of Vibration, Acoustics, Stress, and Reliability in Design, Vol. 105, Issue 2 (1983), pp. 253-260.

Granger, S., and Paidoussis, M. P., An improvement to the quasi-steady model with application to cross-flow-induced vibration of tube arrays, Journal of Fluid Mechanics, Vol. 320, August 1996. pp. 163-184.

Ichioka, T., Kawata, Y., Nakamura, T., Izumi, H., Kobayashi, T., and Takamatsu, H., Research on fluid elastic vibration of cylinder arrays by computational fluid dynamics: analysis of two cylinders and a cylinder row, JSME International Journal, Series B, Vol. 40, No.1 (1997). pp. 16-24.

Kassera, V., and Strohmeier, K., Simulation of tube bundle vibrations induced by cross-flow, Journal of Fluids and Structures, Vol. 11, No.8 (1997), pp. 909-928.

Khulief, Y. A., Al-Kaabi, S. A., Said, S. A., and Anis. M., Prediction of flow-induced vibrations in tubular heat exchangers. Part I: Numerical modeling, ASME Journal of Pressure Vessel Technology, Vol. 131, February 2009, p. 011301.

Lever, J. H., and Weaver, D. S., A theoretical model for fluid-elastic instability in heat exchanger tube bundles, ASME Journal of Pressure Vessel Technology, Vol. 104, August 1982, pp. 147-158.

Mureithi, N. W., Zhang, C., Ruel, M., and Pettigrew, M. J., Fluidelastic instability tests on an array of tubes preferentially flexible in the flow direction, Journal of Fluids and Structures, Vol. 21, No.1 (2005), pp. 75-87.

Paidoussis, M. P., A review of flow-induced vibrations in reactors and reactor components, Nuclear Engineering and Design, Vol. 74, No.1 (1983), pp. 31-60.

Price, S. J., A review of theoretical models for fluidelastic instability of cylinder arrays in cross-flow, Journal of Fluids and Structures, Vol. 9, No. 5 (1995), pp. 463-518.

Price, S. J., and Paidoussis, M. P., An improved mathematical model for the stability of cylinder rows subject to cross-flow, Journal of Sound and Vibration, Vol. 97, No. 4 (1984), pp. 615-640.

Tanaka, H., Tanaka, K., Shimizu, F., and Takahara, S., Fluidelastic analysis of tube bundle vibration in cross-flow, Journal of Fluids and Structures, Vol. 16, No.1 (2002), pp. 93-112.

Violette, R., Mureithi, N. W., and Pettigrew, M. J., Two-phase flow induced vibration of an array of tubes preferentially flexible in the flow direction, In: Pettigrew, M. J., Mureithi, N. W. (Eds.), Flow Induced Vibration 2005, ASME, New York, paper No. PVP2005-71001.

Weaver, D.S., and Grover, L. K., Cross-flow induced vibrations in a tube bank—turbulent buffeting and fluid elastic instability, Journal of Sound and Vibration, Vol. 59, No.2 (1978), pp. 277-294.

Weaver, D. S., Ziada, S., Au-Yang, M. K., Chen, S. S., Paidoussis, M. P., and Pettigrew, M. J., Flow-induced vibrations in power and process plant components—progress and prospects, ASME Journal of Pressure Vessel Technology, Vol. 122, August 2000, pp. 339-348.

Yetisir, M., and Weaver, D. S., An unsteady theory for fluidelastic instability in an array of flexible tubes in cross-flow. Part I: Theory, Journal of Fluids and Structures, Vol. 7, No.7 (1993), pp. 751-766.

Yetisir, M., and Weaver, D. S., An unsteady theory for fluidelastic instability in an array of flexible tubes in cross-flow. Part II: Results and comparison with experiments, Journal of Fluids and Structures, Vol. 7, No.7 (1993), pp. 767-782.

[DOI: 10.1299/mej.14-00377]